communications earth & environment

Article

https://doi.org/10.1038/s43247-024-01311-z

Deep-ocean channel-wall collapse order of magnitude larger than any other documented

Adam D. McArthur [1] ✉, Daniel E. Tek[1], Miquel Poyatos-Moré[2], Luca Colombera[3] & William D. McCaffrey[1]

Submarine channels are the largest conveyors of sediment on Earth, yet little is known about their stability in the deep-ocean. Here, 3D seismic data from the deep-ocean Hikurangi channel-levee system, offshore New Zealand, reveal the largest channel-wall failure yet documented. Collapse of both channel-walls along a 68 km stretch created a mass-transport deposit of 19 km^3, containing 4 km long blocks. Channel-walls typically collapse piecemeal, but here synchronous failure of both channel-walls and landslide erosion of the seafloor is documented, requiring a new process model for channel-wall failure. Mass-failure on this scale poses an under-appreciated risk to seafloor infrastructure both within channels and over regions extending twice the channel width into their overbank. Hitherto, channel-wall failures of this size are unrecognised in abyssal plains; its scale changes our understanding of how channel-levee systems are constructed and how they conduct sediment, carbon and pollutants into the deep-ocean.

Submarine channels transfer and deposit great volumes of sediment, organic matter and pollutants into and within the oceans[1,2]. In contrast to rivers, where localised, small-scale channel-wall collapse is documented to be an important morphodynamic process[3], and a source of geohazard[4], the scale, dynamics, causes and implications of wall collapse processes in submarine channels are poorly understood. Uncertainties remain, therefore, regarding geohazard assessment for seafloor infrastructure, and the impact of submarine channel-wall collapses on global fluxes of sediment, organic carbon and pollutants through the deep-sea.

Submarine canyons incising the continental shelf typically transition downstream into aggradational submarine channels on continental slopes and basin floors[5], where flows overspilling from the channel form overbank deposits, primarily levees[6,7]. Depending on their scale, landslide deposits from canyon or channel-wall collapse can occlude or block these conduits, thereby modifying the flux of sediment, carbon and pollutants to the deep sea[8,9]. Further, the triggers and dynamics of their emplacement are important considerations in the assessment of geohazards[10]. Levee-collapse deposits have previously been described as small-scale, recording local failures of channel walls and their levee[10–16] (cf. subaqueous landslides such as continental shelf or slope collapse, which can remobilise thousands of cubic kilometres of sediment[17]). However, the upper size limit of deep-water channel-levee failures, their emplacement mechanisms and implications of large-scale channel-wall collapse remain poorly constrained.

Here we interpret 3D seismic reflection data from the deep-ocean (presently ~2900 m below sea-level) Hikurangi channel-levee system, offshore New Zealand[18] (Fig. 1A, B), to document a channel-levee collapse that, to the best of our knowledge, is orders of magnitude larger than any other previously reported. Although channel-wall collapses have been studied in proximal slope canyons and channels[10–16], the sparsity of data from deep-ocean channels means the nature of channel-levee collapses in the deep-sea remains ambiguous. Morphometric analysis of the resultant mass-transport deposit (MTD) documents how this example differs from those in continental slope settings, and warrants a new model for the process of large-scale leveed channel-wall failure. The recognition of this new scale of channel-wall failure changes our understanding of how deep-ocean channel-levee systems are constructed, sequester sediment including organics and pollutants, and highlights new implications for the evaluation of submarine landslide geohazards.

Hikurangi channel-levee system

The Hikurangi Channel sits within the southwest-northeast trending Hikurangi Trench[18], where water depths presently range from 2600–3600 m (Fig. 1B). Most of the sediments filling the trench are <3.5 Ma[19] and comprise pelagic, turbidite, contourite and mass-transport deposits[20]. Sediment derived from the South and North Islands enters the trench via slope traversing canyons[21] (Fig. 1B) and is dispersed along-trench via the Hikurangi

[1]School of Earth and Environment, University of Leeds, Leeds, UK. [2]Departament de Geologia, Universitat Autònoma de Barcelona, Cerdanyola, del Vallés, Spain. [3]Department of Earth and Environmental Sciences, University of Pavia, Pavia, Italy. ✉e-mail: A.McArthur@leeds.ac.uk

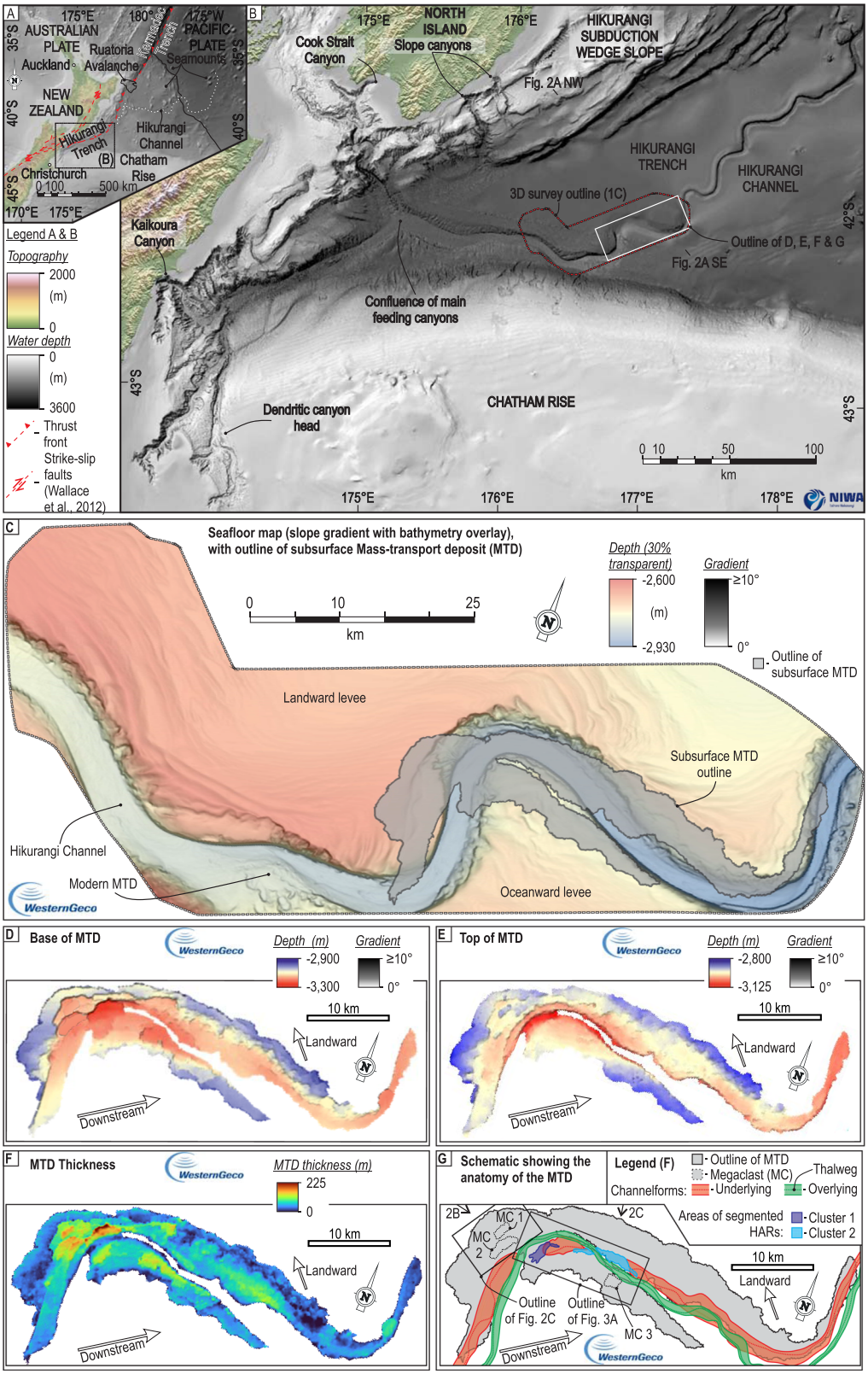

Fig. 1 | Location of the study area and mapped extent of the documented mass-transport deposit (MTD). A Map showing the Hikurangi Channel in relation to the plate-scale features. **B** Map of the proximal reach of the Hikurangi Channel. Bathymetry courtesy of the New Zealand National Institute for Water and Atmosphere. **C** Seafloor expression of the modern Hikurangi Channel within the 3D survey area, with outline of subsurface MTD annotated. **D** Dip map with depth overlay showing the base of the mass-transport deposit (MTD). **E** Dip map with depth overlay showing the top of the MTD. **F** Map showing the thickness of the MTD. **G** Map showing the schematic arrangement of the MTD, with the location of the underlying and overlying channel-forms.

Channel. At 100–200 km from the canyon heads, a confluence of the feeding canyons occurs (Fig. 1B). This study focuses on a portion of the channel-levee system a further 100 km downstream of this confluence, on the deep-ocean floor (Fig. 1B).

Within the survey area, the shallowest 500 m of trench-fill does not contain any sediment remobilised en-masse from the adjacent continental slope[22]. There is no evidence that mass-wasting from either the New Zealand continental shelf or slope, nor from the Chatham Rise delivered landslides to this area of the trench[8], which is situated tens of kilometres from the closest break of slope (Figs. 1A and 2A). Rather, relatively fine sediment is transported axially along the channel, overspilling to form the overbank successions that extend towards both the Chatham Rise and the subduction wedge (Fig. 2A).

The channel system comprises sand-rich channel-fills, heterolithic terrace deposits and MTDs, laterally bounded by heterolithic levee deposits[18] (Fig. 2A–C). The channel has been aggradational since the Pleistocene[19], building low-angle external levees, which taper into the background trench-fill[7]. The observations presented herein build upon an extensive interpretation framework[7,8,18,20–23], which allowed all the aggradational channel-forms and their contemporaneous overbank sequences to be mapped. Channel-fills occur in a stacked, sequentially-active series, each of which follows a modified, but similar, path to its precursor, akin to the path of the presently active seafloor channel (Fig. 2A).

Results

Channel-levee failure mass-transport

A predominantly chaotic interval is associated with one channel-form, the base of which sits at ~400 m below the seabed (Fig. 2A), interpreted as a well-preserved MTD. This MTD is present across the eastern portion of the dataset (Figs. 1 and 2). The elongate geometry of the MTD roughly follows the path of the underlying and overlying channel-forms (Fig. 1G). The MTD is continuous along-channel for 68 km, covers >340 km^2 and has a preserved volume of ~19.3 km^3 (Fig. 1F; Table 1).

The MTD is thickest around the second major meander bend of the channel system, tapering gradually both up- and downstream, and in all directions away from the channel (Fig. 1F). An elongate thin zone corresponding to the path of the overlying channel-form that incises the MTD runs along the axis of the deposit (Figs. 1F, G and 2B, C). The channel-form associated with the MTD is well-preserved up- and downstream of the MTD and displays no evidence of mass-transport bypass (e.g., drag marks from megaclasts) or the passage of a substantial mass-transport event[8], showing that the MTD was locally derived and not introduced axially.

The MTD spans the ~2.5 km width of the underlying channel-form, and extends onto overbank areas on both sides of the channel-form for up to 5 km away from the channel margins, terminating against a series of connected, scallop-shaped indentations (Figs. 1F and 2B, C); beyond this, there is no trace of the MTD or associated erosion, confirming that it was locally sourced. In overbank areas corresponding to the location of the pre-failure external levees (*sensu* Tek et al.[8]), the MTD overlies: (a) Flat, <10 km^2 platforms dipping in accordance with the underlying overbank stratigraphy, typically located along peaks (black reflectors), which are interpreted as mechanically weak layers (Fig. 3B). (b) Steep (up to ~80°) steps that link adjacent flat platforms, against which adjacent overbank reflectors terminate; in plan-view, most are gently curved, up to 5.7 km long, and are oriented subparallel to the channel-form (Figs. 1D and 3B); some shorter (up to 4 km long), relatively straight, channel-subperpendicular steps connect laterally offset channel-subparallel stretches (Figs. 1D and 3B).

Where the MTD overlies terrace deposits (*sensu* Tek et al.[8]), its base conforms to the terrace-bounding surfaces, i.e., dipping up to ~20° toward the channel (Fig. 2C). Steps at the outermost MTD margins transition into <75 m high terrace-bounding surfaces against which overbank sediments from younger channel-forms terminate (Figs. 2B and 3C), which represent the relief created by MTD emplacement. Such surfaces indicate the area of full MTD evacuation was limited to the scallop-shaped indentations and that the MTD was locally generated.

The MTD itself is imaged as chaotic to transparent packages, folded and faulted reflectors, and as blocks of coherent reflectors surrounded by chaotic seismic facies (Fig. 2B, C). The dominant MTD seismic facies comprises chaotic reflectors with little internal reflectivity (Figs. 2B, C and 3B–D). These chaotic reflectors are interpreted as slump and debris-flow material sourced from shallower overbank stratigraphy (Figs. 2C and 3D). Undeformed or weakly-deformed blocks of reflectors separated from the overbank reflectors by chaotic packages, but with similar seismic character as the adjacent in-situ overbank are interpreted as megaclasts (Fig. 3A–D).

The megaclasts can be up to 120 m thick, 4.1 km long, and have surface areas up to 3.9 km^2 (Table 1, Fig. 3A). Although there are numerous megaclasts, they exhibit two distinct styles as represented by the three largest megaclasts:

(1) Megaclast 1 (MC1) and Megaclast 2 (MC2) lie adjacent to the left bank of the channel (Figs. 1G, 2B and 3A). They exhibit similar dip and reflector sequences to the nearby in-situ overbank (Figs. 2B and 3B). In plan-view, their long edges are sub-parallel to the strike of steps in the failure surface, and their corners match to kinks in these steps (Fig. 3B), suggesting that the blocks were locally sourced by retrogressive failure of the channel-wall and slid along decollement surfaces parallel to the orientations of overbank strata.

(2) Megaclast 3 (MC3) sits further downstream, adjacent to the right bank (Fig. 1G). The base of this megaclast mirrors the curvature of the MTD-bounding surface, which shallows toward the thickest part of the MTD, a geometry resembling a terrace-bounding surface; reflectors within MC3 dip towards this surface (Fig. 2C). Between and on top of the megaclasts, wedges of chaotic material are thickest where the top of the megaclast meets the MTD base and thin towards and away from the channel-form (Fig. 3D). MC3 is interpreted as a rotated slide block that potentially represents pre-existing terrace deposits that slid along a weak terrace-bounding surface.

The style of megaclast emplacement was likely determined by the nature of the pre-failure stratigraphy.

For most of its length, the MTD overlies a ~40 m thick, up to 2.5 km wide sequence, imaged as high amplitude reflectors (HARs) nested in a concave-up surface, interpreted as sand-rich deposits of the underlying channel-form[8] (Fig. 2C). However, these deposits are absent beneath the thickest parts of the MTD (Figs. 2B and 3E). Instead, imbricate blocks of HARs are seen laterally, encased by chaotic deposits (Fig. 3F, G). The HAR stacks are up to 40 m thick, 1.5–7 km^2 in area and dip up to 50° toward the thickest part of the MTD (Figs. 2B, C and 3E–G). These HARs are interpreted as shingled units of channel-floor deposits, ripped up from their original locations and forced onto the channel margin opposite to the failure source (Fig. 4). These occur in two distinct clusters: (1) adjacent to the maximum thickness of the MTD, where the thrust geometries suggest a transport direction to the SE toward the oceanward channel margin (Fig. 3E, F), and (2) adjacent to the downstream landward channel margin, where thrusts suggest NE transport (Fig. 3E, G). At the upstream end of cluster 1, there is a 700 m long stretch where no HARs are present under or within the MTD (Fig. 3E). Here, the underlying HARs appear to have been ripped up and transported down-channel. Imbrication of the upstream HAR cluster (1) to the SE is interpreted to result from failure of the left channel-wall eroding and deforming strata. Imbrication of the downstream HAR cluster (2) to the NE is interpreted to result from failure of the right channel-wall.

The erosional nature of the MTD indicates that the volume of displaced materials exceeded that of the initial failure. The entire MTD top is incised by a post-failure channelform locally scouring to the MTD base (Fig. 1E, F), indicating that the original composite size of the MTD exceeded the preserved volume. *Loci* of subsequent channel erosion correspond to topographic lows on the original MTD surface (Fig. 5).

Comparison with other channel-wall failure MTDs

To assess the importance of the studied channel-wall failure MTD, data on the morphometry of MTDs contained in other submarine channel-fills

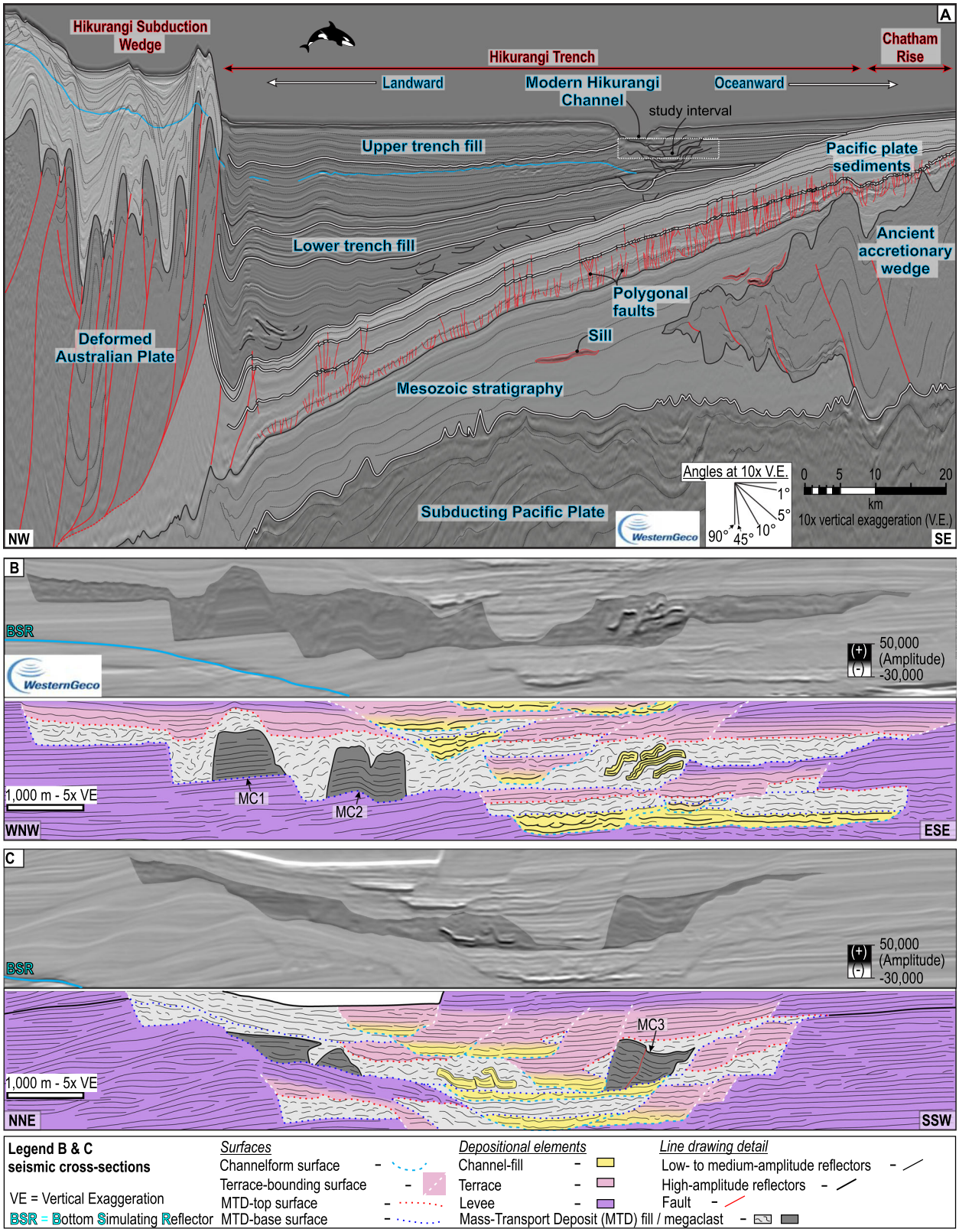

Fig. 2 | Cross-sections of the Hikurangi Trench, Channel and the mass-transport deposit. A Interpreted cross-section of the Hikurangi Trench, from the Hikurangi subduction wedge to the Chatham Rise, modified from McArthur and Tek[22]. **B** Uninterpreted and interpreted seismic cross-sections intersecting the MTD upstream of the first meander bend. **C** Uninterpreted and interpreted seismic cross-sections intersecting the MTD downstream of the first meander bend. See Supplementary Fig. 1 for non-interpreted versions.

Table 1 | Volumes and areas of the mass-transport deposit (MTD) and three largest megaclasts

	Maximum thickness (m)	Median thickness (m)	Maximum long-axis length (m)	Area (m^2)	Volume (m^3)
Wall-collapse MTD	265	50		340828165	19267539760
Megaclast 1	141	120	2400	1933116	169916285
Megaclast 2	136	115	4080	3902347	341396797
Megaclast 3	130	105	2760	2767878	257922000

See Supplementary Material 1 for information on other channel-wall collapse MTDs.

documented in the scientific literature (Supplementary Table 1) and stored in the Deep-Marine Architecture Knowledge Store (DMAKS[24]) have been compiled (see Supplementary Note for details).

A comparison between the morphometry of the studied channel-wall failure MTD and that of other examples of intra-channel MTDs demonstrates that the scale of the studied MTD is far greater than any of the analogous MTDs previously documented (Fig. 6), confirming its exceptional nature. Although practically all the other examples document failures in canyon to slope channels, these are the most comparable failures to the deep-ocean example documented here.

Discussion and implications

Processes of giant deep-ocean channel-wall failure

Mapping of the MTD, its contacts with bounding reflectors and analysis of its associated kinematic indicators permit interpretation of the MTD sources (Fig. 4A). To date MTDs of this size have been interpreted to originate only from shelf or slope failures[25–27], yet the studied MTD originated locally at the walls of a deep-ocean channel.

Mapping of the contemporaneous overbank succession beyond the failure found no hint of the MTD, or erosional features related to MTD bypass[7]. Given the distance from both the Hikurangi subduction wedge (~50 km distant) and much gentler Chatham Rise slope (~20 km) the studied MTD could not have originated from coeval shelf or slope collapses (Fig. 1A). There are no tectonic structures in this region of the abyssal plain from where the landslide could have originated (Fig. 1B). The lack of evidence for this MTD in upstream channel sections also discards that it could it have been sourced axially from or through contemporaneous slope canyons[8].

The scalloped landward margin on the upstream portion of the channel is identified as the lateral boundary of the primary failure area (Figs. 1F, 3A–C, 4A, B), which sits ~5 km laterally away from the pre-failure channel-form margin (Fig. 1F). Therefore, the source areas of the failure are clearly imaged and constrained, demonstrating that it originated locally at the walls of the channel (Fig. 3A–D). The scallops are interpreted as headwall scarps, and thus MTD erosion extended laterally for up to 5 km (ca. twice the channel width) into the pre-failure overbank succession. Downward steps towards the channel axis are interpreted as ramps in the basal shear plane. The stratigraphic levels of the decollements were likely determined by sediment lithology and pore pressures[28]. The megaclasts were detached from nearby steps as new up-dip ramps initiated, sliding across the underlying decollements via a mechanism similar to 'lateral spreading'[29]. These megaclasts originated at different stratigraphic levels; they were encased in chaotic deposits mobilised from higher stratigraphic levels whilst the megaclasts were moving (Figs. 2B, 3A–C and 4A, B).

A second failure area is identified on the oceanward margin, in the downstream portion of the channel, also exhibiting scalloped headwall scarps (Figs. 3D and 4A, C). Here a failure plane likely exploited a mechanically weak surface at the boundary between terrace and levee[8] (Fig. 2C), such that the associated megaclast 3 rotated as it detached. The absence of growth strata on or next to megaclasts in the subsequent channel-fill suggests that the failure happened quasi-instantaneously. That the pre-existing channel-fill HAR was eroded, transported both across and down-channel to form imbricate stacks speaks to the energy involved in this scale of mass-failure, which is in contrast to existing models of piecemeal channel-wall collapse[14].

Implications of simultaneous collapse of both channel-walls

The coalesced fabric of the MTD implies that failures 1 and 2 were essentially coeval, with both channel flanks collapsing contemporaneously (Fig. 5). Deposits from the failure are preserved on both sides of the channel-form, with the low point of the MTD top inferred to have been in the middle of the MTD, between material derived from the failed stratigraphy, and material that ran up the opposite channel margin. Subsequent channel flows were focused between megaclasts and imbricated HARs where both were present (Fig. 5). If the failure had affected only one margin, the deposits would have been preferentially stacked at one flank, whilst subsequent turbidity currents would have preferentially eroded the MTD toes, limiting MTD preservation across the channel[12].

The MTD architecture implies synchronous failure of both channel-walls. However, it is not possible to determine whether both failures were triggered simultaneously, or whether one failure triggered the other (Fig. 4). Channel-wall failures are typically interpreted to result from undercutting and destabilisation by channel flows[12,13,17,30,31]. In such cases, the resulting MTD is normally spatially restricted, partially filling but not blocking the channel, and will ultimately be cleared by subsequent flows[12]. In the studied example, the simultaneous failure of both channel-walls along tens of kilometres would have blocked the channel (Fig. 5). Where a channel is superelevated above surrounding areas such blockages could lead to avulsion of subsequent channel-traversing flows[16]. This did not occur here, as the wider confinement of the trench enabled aggradation of the overbank sequence to keep pace with that of the channel aggradation; as channel superelevation remained modest, the channel axes up- and down-stream of the MTD location remained below the level of the contemporaneous overbank, inhibiting flow breakout.

It is particularly novel that the failure originated within the channel and >100 km from the base of slope canyon confluence on the abyssal plain (Fig. 1A), rather than being externally sourced. Recognising that such large events can be generated by deep-ocean channel-levees fundamentally changes our understanding of how deep-water channel systems, the greatest conveyors of sediment on Earth[5], function on the abyssal plain.

Implications for sediment, pollutant and carbon fluxes through deep-ocean channels

The topography generated by the studied MTD controlled the location of re-incision and channel formation post-MTD emplacement, which exploited the lowest path across the top of the deposit (Figs. 2B, C and 5). This means that channel-wall collapse MTDs can control the stacking of deep-water channel deposits. Hence, the emplacement of channel damning MTDs may significantly alter the sediment flux through channels, including trapping large volumes of sediment upstream of the failure[8]. In the example studied here, MTD damning trapped at least 19 km^3 of sediment, including organic carbon, in the channel system, rather than its delivery to the terminal submarine fan.

Recent work from the Congo Canyon revealed that ~0.4 km^3 of sediment containing ~5 Mt of organic carbon was sequestered upstream of a ~0.9 km^3 landslide dam[9]. Evidence for the failure of steep canyon walls in the most proximal parts of submarine canyon and slope channel systems is common[32], suggesting landslide damming and subsequent erosion may be a major control on the flux of sediment organic carbon and pollutants to the deep sea. However, due to a paucity of observations of wall-collapse deposits in deep-ocean channels, uncertainties remain regarding impact of this process the deeper-water parts of channel systems, which are typically much

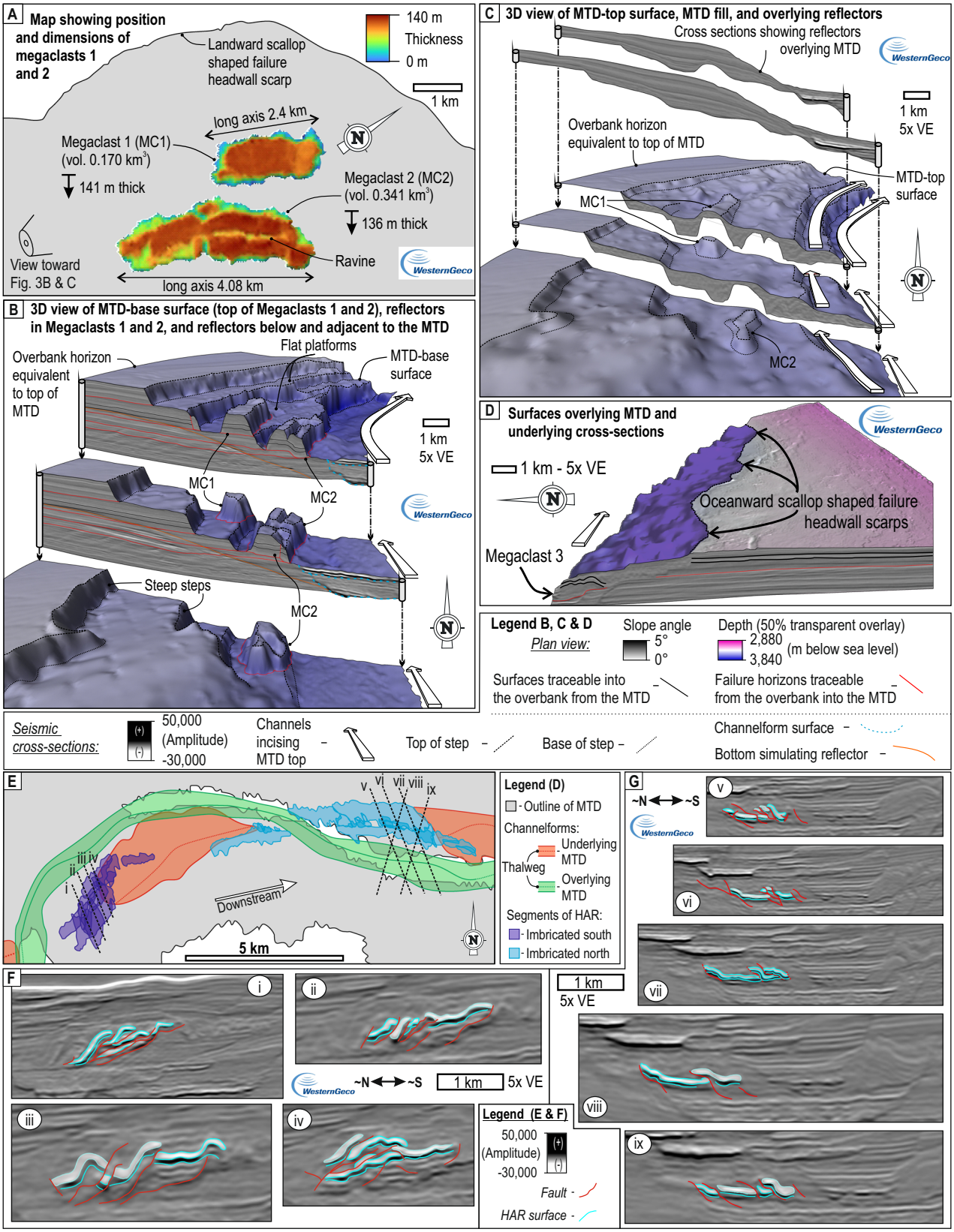

Fig. 3 | 3D views of megaclasts and remobilised channel-fill cross-sections. **A** Thickness map of megaclasts 1 and 2 (within the outline of the MTD top), with long-axis length, maximum thickness, and volume annotated. **B** 3D diagram showing the nature of the upstream landward contemporaneous overbank surface, source area and MTD top. **C** 3D diagram showing the nature of the upstream landward contemporaneous overbank surface, source area and failure surfaces. **D** 3D diagram showing the nature of the oceanward contemporaneous overbank surface, source area and failure. **E** Distribution map of rip-up high amplitude reflectors (HARs), on both channel margins. **F** Sections i to iv through upstream cluster of rip-up HARs. **G** Sections v to ix through downstream cluster of rip-up HARs. See Supplementary Fig. 2 for non-interpreted versions of **F** and **G**.

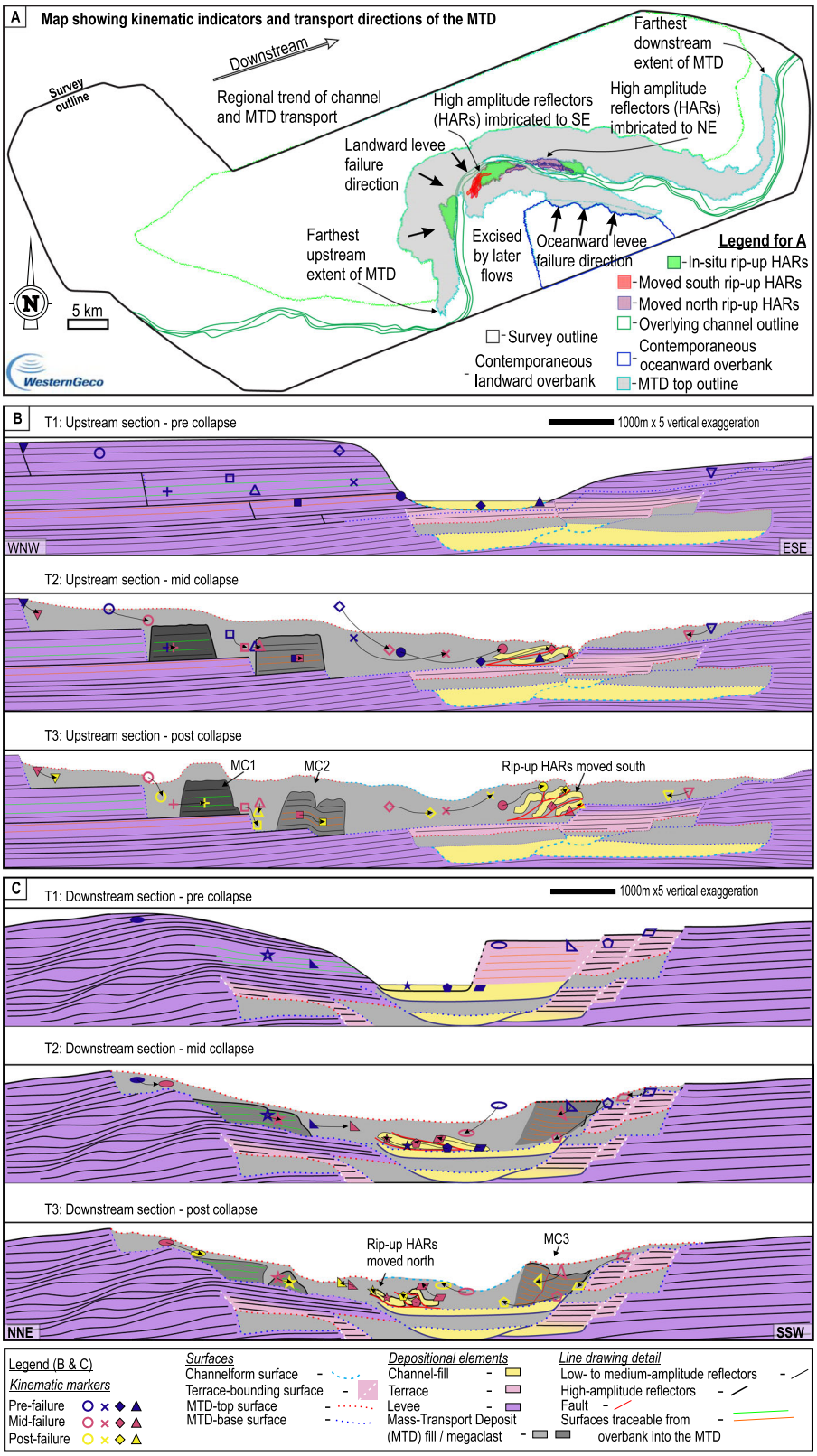

Fig. 4 | Process model of the channel-wall landslide. A Map showing the kinematics and general directions of movement in the different parts of the MTD, with arrows showing megaclast failure directions; contemporaneous landward source area, upstream cluster of rip-up HARs, downstream cluster of rip-up HARs, and oceanward source area. **B** Evolution of failure at the upstream location (Fig. 2A), through three timesteps. **C** Evolution of failure at the downstream location (Fig. 2B), through three timesteps.

longer and sequester more sediment than their feeding canyons[21]. Here, to the best of our knowledge, this process of channel-wall failure MTDs damning a channel is documented for the first time in deep-ocean channels, indicating this process is not restricted to the canyon-confined proximal parts of deep-water sedimentary systems, but is more widespread than presently recognised.

Furthermore, the wall-collapse studied here shows that a large, steep canyon wall (cf. the 800 m deep Congo Canyon) is not necessary to generate large wall-collapse MTDs that could dam a channel. Estimates of the relief derived from the deposit's failure scars (<75 m high) suggest the <265-m-thick MTD studied here, was generated from the collapse of channel-walls not much larger than the deposit's maximum thickness. Hence, MTDs

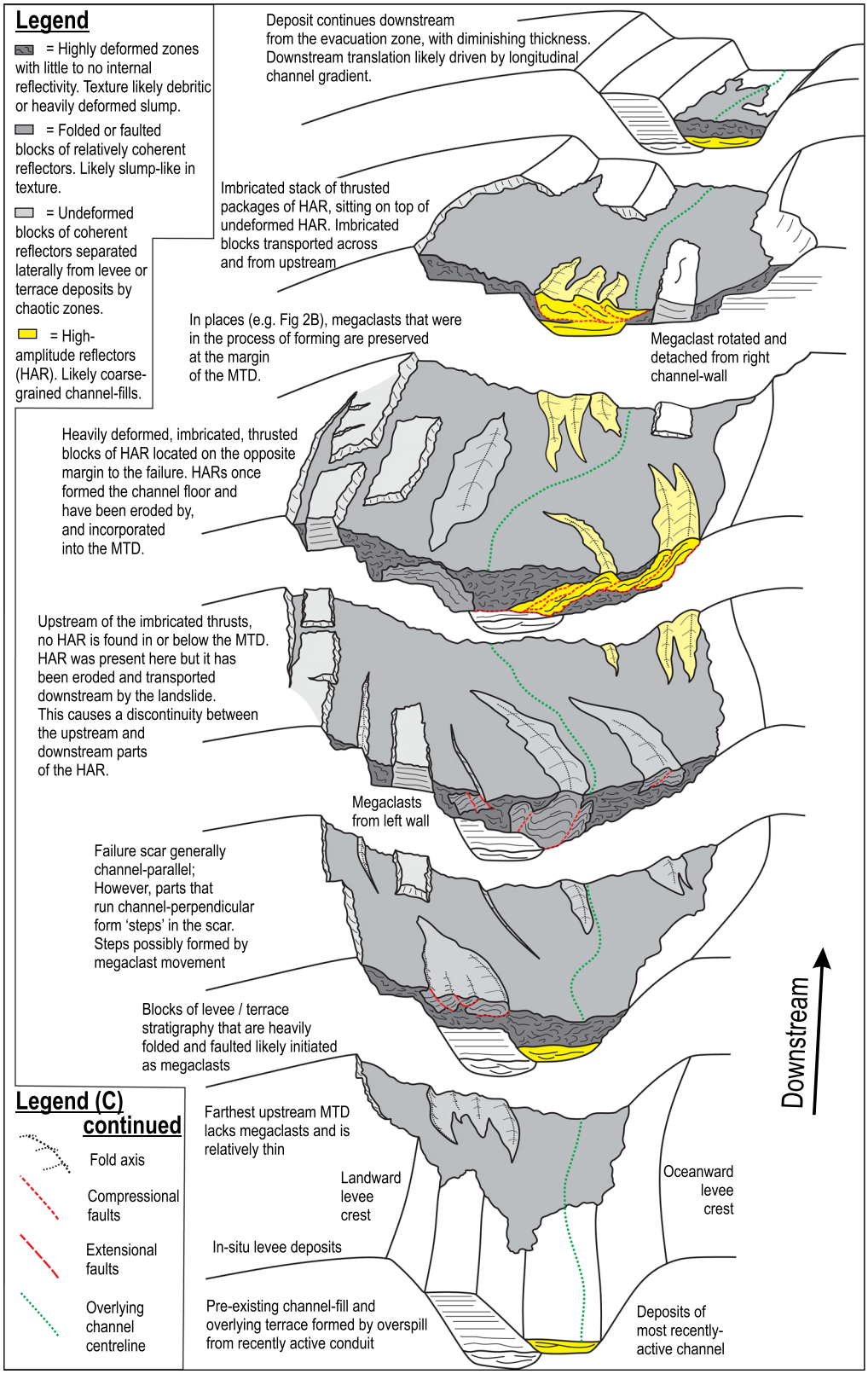

Fig. 5 | 3D diagram showing schematically how simultaneous collapse of both channel-walls results in complicated 3D MTD distribution and MTD top topography. A series of cross-sections and channel-levee morphometry is shown from upstream to downstream of the MTD.

almost as thick as the channel-walls from where they were derived could trap sediment and modify the flux of sediment, carbon and pollutants over thousands of kilometres along the levee bound stretches of aggradational deep-ocean channels.

Implications for channel-wall collapse geohazards

The mass-failure documented here eroded and remobilised existing channel-fill at a scale not previously recognised. The size of levee collapse needed to destabilise both channel margins simultaneously and to erode the

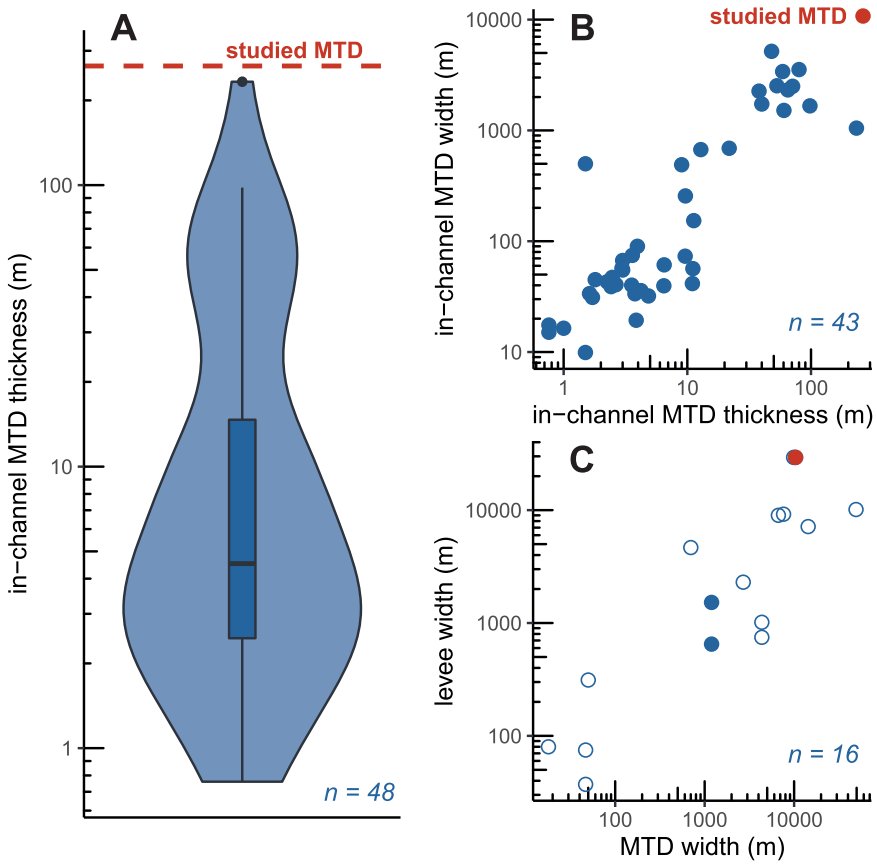

Fig. 6 | Morphometry of mass-transport deposits contained within channels and/or spatially related to levees, and documented in the literature case studies included in the study database (see supplementary material). A comparison is made between the studied MTD and other known examples in terms of **A** MTD thickness, **B** MTD width-to-thickness scaling, and **C** relative cross-channel widths of MTDs and associated channel-levees. In **A**, the box plot represents the interquartile range, the horizontal bar represents median values, and the dot represents an outlier (value larger than 1.5 times the interquartile range); the violin plot represents kernel density. In **C**, empty spots denote MTDs that are not contained within channel elements, i.e., which are located in the outer part of levees, recording failure away from the parent channel.

pre-existing channel-fill is consistent with an interpretation of quasi-instantaneous MTD emplacement (cf. incremental failure[14], or an amalgamation of smaller slumps and slides as invoked to explain other levee-collapses[12]). As previous studies all invoke isolated, small-scale failure of a channel-wall, with no erosion of the channel-floor, the studied MTD therefore necessitates the development of a new process model of large-scale channel-levee collapse (Fig. 4); in parallel, the erosive potential of failures of such magnitude represents a previously unrecognised submarine geohazard.

Placement of infrastructure within channels is already considered hazardous, due to the activity of channel-traversing turbidity currents[33], and to small-scale channel-wall failures[34]. Yet the potential for large-scale channel-wall collapse represents an additional risk in terms of seafloor deformation; in particular, the plucking of rafts of channel-floor stratigraphy many tens of metres thick and their transportation for hundreds of metres represent a substantial hazard to infrastructure located on or under the channel floor. The MTD emplacement studied here caused the excavation of material to a depth of at least 40 m (cf. local erosion depths by turbidity currents of up to 20 m[35]), indicating that safety thresholds for safe burial should be extended to safeguard against MTD hazards in similar settings.

While placement of infrastructure on channel overbank areas might be deemed safer than in the channel itself, we document that large-scale channel-wall collapse events may remobilise overbank deposits at least twice the channel width away from their associated channel margin. This represents a serious, and to the best of our knowledge, hitherto unforeseen risk to infrastructure located in overbank areas, previously considered theoretically safely away from unstable channel margins. Safe planning guidelines should be amended to consider this risk.

The largest channel-wall failure ever documented

This is the largest channel-wall failure ever documented (Fig. 6). More remarkably, channel-wall failures that have been previously reported are all contained on submarine slopes within tens of kilometres of their canyons heads, excepting the Zaire fan[36], rather than the abyssal plain as in this study; such large failures are therefore seemingly rare. Nevertheless, several lines of argument suggest that other examples of failures of this scale may have gone unrecognised:

- Firstly, MTDs such as those described here are difficult to identify in outcrop studies; at 120 m in thickness and 4 km in length the studied megaclasts are larger than most outcrops of channel-levee deposits and may be misinterpreted as in-situ overbank stratigraphy. Deformed stratigraphy or imbricated thrusts separating packages tens of metres thick over several square kilometres may be misinterpreted as tectonic in origin.
- Secondly, erosion by subsequent flows may remove a greater proportion of the MTD than is documented here, where the studied MTD has good preservation. Other large examples may have been eroded to such an extent that their original scale is unknown.
- Thirdly, the MTD documented here is imaged in a high-resolution and large-scale 3D seismic data set. It may be very difficult to resolve such deposits in poorer quality, less extensive 3D or 2D seismic data. In particular, 3D seismic surveys of deep-ocean channels are very rare.
- Finally, the scale of failure presents challenges to its recognition in wireline well data, or in core.

As such, the likelihood of such large-scale collapses of channel and overbank stratigraphy may be under-recognised, and the associated risks underestimated. This is the case even in the deep-ocean, where such failures may occur at great distances (here >100 km) from the nearest continental slopes, from where large failures are typically considered to originate.

Data and methods

2600 km^2 of pre-stack Kirchoff depth migrated (broadband) 3D seismic data covering a 150 km long stretch of the Hikurangi Channel (Fig. 1) were

studied. Full-stack data show a downward increase in acoustic impedance as a trough (white reflection). The horizontal resolution of the survey is ~25 m and the vertical resolution is ~7 m[37].

Seismic interpretation, horizon mapping, surface extraction and attribute analysis were conducted in SLB's Petrel, following a standard framework[8]. The top and base of the studied MTD were mapped (Fig. 1C, D), and its minimum volume calculated (Fig. 1E). Structures in the MTD and adjacent overbank were mapped to characterise the MTD and to identify kinematic indicators.

Data availability

Data collated regarding other channel-levee failure mass-transport deposits can be accessed here: https://doi.org/10.6084/m9.figshare.25053242.v1. Seismic Data provided by WesternGeco (https://www.slb.com/products-and-services/innovating-in-oil-and-gas/reservoir-characterization/seismic/multiclient-data-library) may be obtained by contacting SLB.

Received: 4 August 2023; Accepted: 7 March 2024;
Published online: 19 March 2024

References

1. Rabouille, C. et al. Carbon and silica megasink in deep-sea sediments of the Congo terminal lobes. *Quat. Sci. Rev.* **222**, 105854 (2019).
2. Pohl, F., Eggenhuisen, J. T., Kane, I. A. & Clare, M. A. Transport and burial of microplastics in deep-marine sediments by turbidity currents. *Environ. Sci. Technol.* **54**, 4180–4189 (2020).
3. Thorne, C. R. & Tovey, N. K. Stability of composite river banks. *Earth Surface Processes Landforms* **6**, 469–484 (1981).
4. Das, B. Stakeholders' perception in identification of river bank erosion hazard: a case study. *Natural Hazards* **58**, 905–928 (2011).
5. Peakall, J. & Sumner, E. J. Submarine channel flow processes and deposits: A process-product perspective. *Geomorphology* **244**, 95–120 (2015).
6. Buffington, E. C. Submarine" Natural Levees". *J. Geol.* **60**, 473–479 (1952).
7. Tek, D. E. et al. Controls on the architectural evolution of deep-water channel overbank sediment wave fields: insights from the Hikurangi Channel, offshore New Zealand. *N. Z. J. Geol. Geophys.* **65**, 141–178 (2022).
8. Tek, D. E. et al. Relating seafloor geomorphology to subsurface architecture: how mass-transport deposits and knickpoint-zones build the stratigraphy of the deep-water Hikurangi Channel. *Sedimentology* **68**, 3141–3190 (2021).
9. Pope, E. L. et al. Carbon and sediment fluxes inhibited in the submarine Congo Canyon by landslide-damming. *Nat. Geosci.* **15**, 845–853 (2022).
10. Klaucke, I., Hesse, R. & Ryan, W. B. Morphology and structure of a distal submarine trunk channel: The Northwest Atlantic Mid-Ocean Channel between lat 53 N and 44 30′ N. *Geological Soc. Am. Bull.* **110**, 22–34 (1998).
11. Deptuck, M. E., Steffens, G. S., Barton, M. & Pirmez, C. Architecture and evolution of upper fan channel-belts on the Niger Delta slope and in the Arabian Sea. *Marine Petroleum Geol.* **20**, 649–676 (2003).
12. Sawyer, D. E., Flemings, P. B., Shipp, R. C. & Winker, C. D. Seismic geomorphology, lithology, and evolution of the late Pleistocene Mars-Ursa turbidite region, Mississippi Canyon area, northern Gulf of Mexico. *AAPG Bull.* **91**, 215–234 (2007).
13. Sawyer, D. E., Flemings, P. B. & Nikolinakou, M. Continuous deep-seated slope failure recycles sediments and limits levee height in submarine channels. *Geology* **42**, 15–18 (2014).
14. Hansen, L. A. et al. Genesis and character of thin-bedded turbidites associated with submarine channels. *Marine Petroleum Geol.* **67**, 852–879 (2015).
15. Jobe, Z. R. et al. Comparing aggradation, superelevation, and avulsion frequency of submarine and fluvial channels. *Front. Earth Sci.* **8**, 53 (2020).
16. Peakall, J., Amos, K. J., Keevil, G. M., Bradbury, P. W. & Gupta, S. Flow processes and sedimentation in submarine channel bends. *Marine Petroleum Geol.* **24**, 470–486 (2007).
17. Collot, J. Y., Lewis, K., Lamarche, G. & Lallemand, S. The giant Ruatoria debris avalanche on the northern Hikurangi margin, New Zealand: Result of oblique seamount subduction. *J. Geophys. Res.* **106**, 19271–19297 (2001).
18. Lewis, K. B. The 1500-km-long Hikurangi Channel: trench-axis channel that escapes its trench, crosses a plateau, and feeds a fan drift. *Geo Marine Lett.* **14**, 19–28 (1994).
19. Ghisetti, F. C., Barnes, P. M., Ellis, S., Plaza-Faverola, A. A. & Barker, D. H. The last 2 Myr of accretionary wedge construction in the central Hikurangi margin (North Island, New Zealand): Insights from structural modeling. *Geochem. Geophys. Geosyst.* **17**, 2661–2686 (2016).
20. Underwood, M. B. Composition of fine-grained sediment in the Hikurangi Trough: Evidence for intermingling among axial gravity flows, transverse gravity flows and margin-parallel ocean currents. *Sedimentology* **70**, 828–864 (2023).
21. Mountjoy, J. J. et al. Earthquakes drive large-scale submarine canyon development and sediment supply to deep-ocean basins. *Sci. Adv.* **4**, eaar3748 (2018).
22. McArthur, A. D. & Tek, D. E. Controls on the origin and evolution of deep-ocean trench-axial channels. *Geology* **49**, 883–888 (2021).
23. Lewis, K. B. & Pantin, H. M. Channel-axis, overbank and drift sediment waves in the southern Hikurangi Trough, New Zealand. *Marine Geol.* **192**, 123–151 (2002).
24. Cullis, S., Patacci, M., Colombera, L., Bührig, L. & McCaffrey, W. D. A database solution for the quantitative characterisation and comparison of deep-marine siliciclastic depositional systems. *Marine Petroleum Geol.* **102**, 321–339 (2019).
25. Ortiz-Karpf, A., Hodgson, D. M., Jackson, C. A. L. & McCaffrey, W. D. Mass-transport complexes as markers of deep-water fold-and-thrust belt evolution: insights from the southern Magdalena fan, offshore Colombia. *Basin Res.* **30**, 65–88 (2018).
26. Normandeau, A., Campbell, D. C., Piper, D. J. & Jenner, K. A. *New evidence for a major late Quaternary submarine landslide on the external western levee of Laurentian Fan* (Geological Society, London, Special Publications, 2019). 477, pp.377–387.
27. McArthur, A. D., Crisóstomo-Figueroa, A., Wunderlich, A., Karvelas, A. & McCaffrey, W. D. Sedimentation on structurally complex slopes: Neogene to recent deep-water sedimentation patterns across the central Hikurangi subduction margin, New Zealand. *Basin Res.* **34**, 1807–1837 (2022).
28. Cox, D. R., Huuse, M., Newton, A. M., Gannon, P. & Clayburn, J. Slip sliding away: Enigma of large sandy blocks within a gas-bearing mass transport deposit, offshore northwestern Greenland. *AAPG Bull.* **104**, 1011–1043 (2020).
29. Wu, N. et al. The formation and implications of giant blocks and fluid escape structures in submarine lateral spreads. *Basin Res.* **33**, 1711–1730 (2021).
30. McHargue, T. R. Seismic facies, processes, and evolution of Miocene inner fan channels, Indus submarine fan. In: *Seismic Facies and Sedimentary Processes of Submarine Fans and Turbidite Systems. Frontiers in Sedimentary Geology*. (eds. Weimer, P., Link, M. H.) 403–413 (Springer, New York, NY, 1991).
31. Dorrell, R. M., Burns, A. D. & McCaffrey, W. D. The inherent instability of leveed seafloor channels. *Geophys. Res. Lett.* **42**, 4023–4031 (2015).
32. Watson, S. J., Mountjoy, J. J. & Crutchley, G. J. Tectonic and geomorphic controls on the distribution of submarine landslides across active and passive margins, eastern New Zealand. *Geological Soc. Lond. Special Publ.* **500**, 477–494 (2020).
33. Paull, C. K. et al. Powerful turbidity currents driven by dense basal layers. *Nat. Commun.* **9**, 4114 (2018).

34. Thomas, S, Hooper, J. & Clare, M. Constraining geohazards to the past: impact assessment of submarine mass movements on seabed developments. In: *Submarine Mass Movements and Their Consequences. Advances in Natural and Technological Hazards Research*, (ed. Mosher, D. C.) 28, 387–398 (Springer, Dordrecht., Netherlands, 2010).
35. Morris, W. R. & Normark, W. R., Sedimentologic and geometric criteria for comparing modern and ancient sandy turbidite elements. In *Deep-Water Reservoirs of the World. GCSSEPM Foundation 20th Annual Research Conference*. (ed., Weimer, P.) 606–628 (SEPM Society for Sedimentary Geology, Houston, Texas, 2000).
36. Droz, L. et al. Architecture of an active mud-rich turbidite system: The Zaire Fan (Congo–Angola margin southeast Atlantic) Results from ZaïAngo 1 and 2 cruises. *AAPG Bull.* **87**, 1145–1168 (2003).
37. Crisóstomo-Figueroa, A., McArthur, A. D., Dorrell, R. M., Amy, L. & McCaffrey, W. D. A new modelling approach to sediment bypass prediction applied to the East Coast Basin, New Zealand. *GSA Bull.* **133**, 1734–1748 (2021).

Acknowledgements

Editor Joe Aslin, Reviewer Mads Huuse and an anonymous reviewer are thanked for their constructive comments. WesternGeco are thanked for providing the seismic data.

Author contributions

A.M., D.T. and W.M. jointly conceived the project. A.M., D.T. and L.C. conducted the analysis. A.M., D.T., L.C., M.P-M and W.M. analysed the data. A.M. and D.T. wrote the first manuscript draft and drafted the figures. All authors discussed results and implications and commented on the manuscript at all stages.

Competing interests

The authors declare no competing interests.

Additional information

Supplementary information The online version contains supplementary material available at https://doi.org/10.1038/s43247-024-01311-z.

Correspondence and requests for materials should be addressed to Adam D. McArthur.

Peer review information *Communications Earth & Environment* thanks Mads Huuse and the other, anonymous, reviewer(s) for their contribution to the peer review of this work. Primary Handling Editor: Joe Aslin. A peer review file is available.